

## PAGE CD4

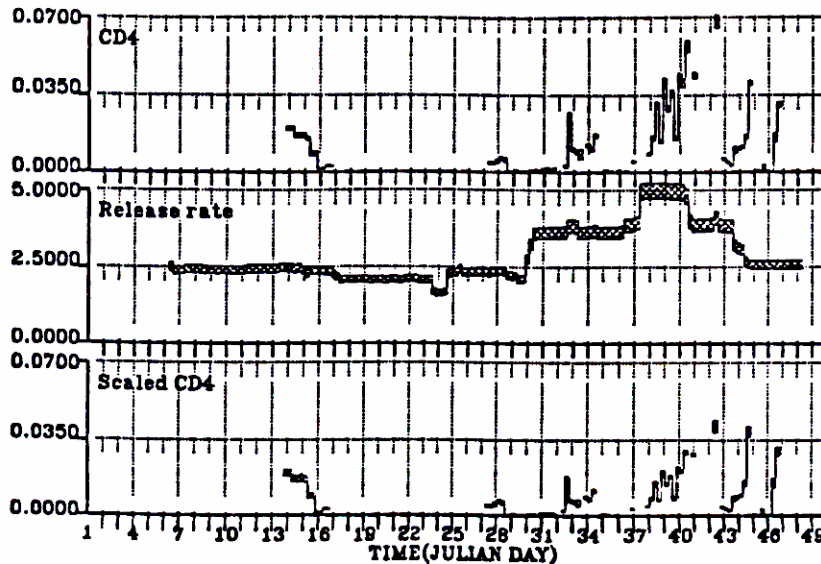


Figure 6.5: Raw  $CD_4$  concentrations (ppt),  $CD_4$  release rate (mg/MWe-h), and  $CD_4$  (ppt) scaled to release rate.

that the release rate from JD = 37.8-40.8 (Unit 3) was indeed higher. The ratio of the  $Se-CD_4$  slope corresponding to JD = 37.8-40.8 (Unit 3) and the lower bound of  $Se/CD_4$  measured in the plume is approximately 0.37; i.e.,  $0.025/0.067 = 0.37$ . Consequently, the  $CD_4$  release rate on JD = 37.8-40.8 is increased by a factor of  $2.7 = 1/0.37$  to account for Unit 3 tracer releases, the resulting  $Se-CD_4$  scatter plot for all data for JD = 27.3-45.3 appears as shown in Figure 6.7. The slope of the least square regression line is  $0.09220 \pm .01$  while the intercept =  $0.00027 \pm 0.00011$  ( $R^2 = 0.69$ ). For the time period corresponding to the high sulfate episode (JD = 37.8-45.3), the slope of the regression line is  $0.089 \pm 0.011$ , the intercept is not significantly different from zero, and  $R^2 = 0.85$ . The slope of either 0.092 or 0.089 is close to the average in-plume measured  $Se/CD_4$  ratio of 0.097 but somewhat higher than the best estimate of 0.067 found in the 10 mile 1/29/87 sample.

Figure 6.8 is temporal plots of ambient  $CD_4$  concentrations, the tracer release rate,  $CD_4$  scaled to NGS's emission rate, the apparent release rate accounting for Unit 3, and  $CD_4$  scaled to the apparent release rate, at the monitoring site for Page. The scaled  $CD_4$  data will be used for the remainder of this report.

## 6.3 Deposition and Transformation Rates

### 6.3.1 Dry Deposition Rates

Dry deposition is the process of mass transfer by which gases and particles are removed from the atmosphere to the surfaces of soil, rock, vegetation, and water bodies. Deposition involves a series of processes starting with atmospheric diffusion to the ground surface followed by various physical, chemical, and biological processes. Hicks<sup>1</sup> provides an excellent overview of the important processes



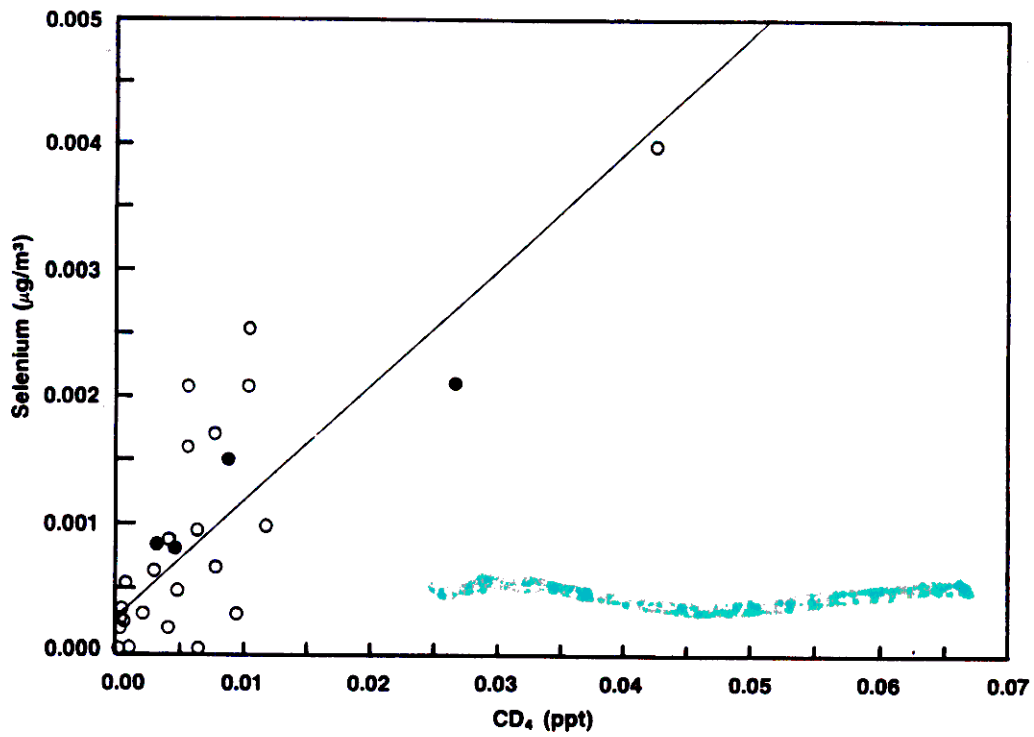


Figure 6.7: Scaled  $\text{CD}_4$  (ppt) plotted against  $\text{Se}$  ( $\mu\text{g}/\text{m}^3$ ). \* corresponds to data gathered on JD = 42.8, 43.3, 43.8 and 44.3. The equation for the regression line is  $\text{Se} = 0.00027 \pm 0.00011 + (0.092 \pm 0.011)(\text{CD}_4)$ .

CD4/S  
3.25

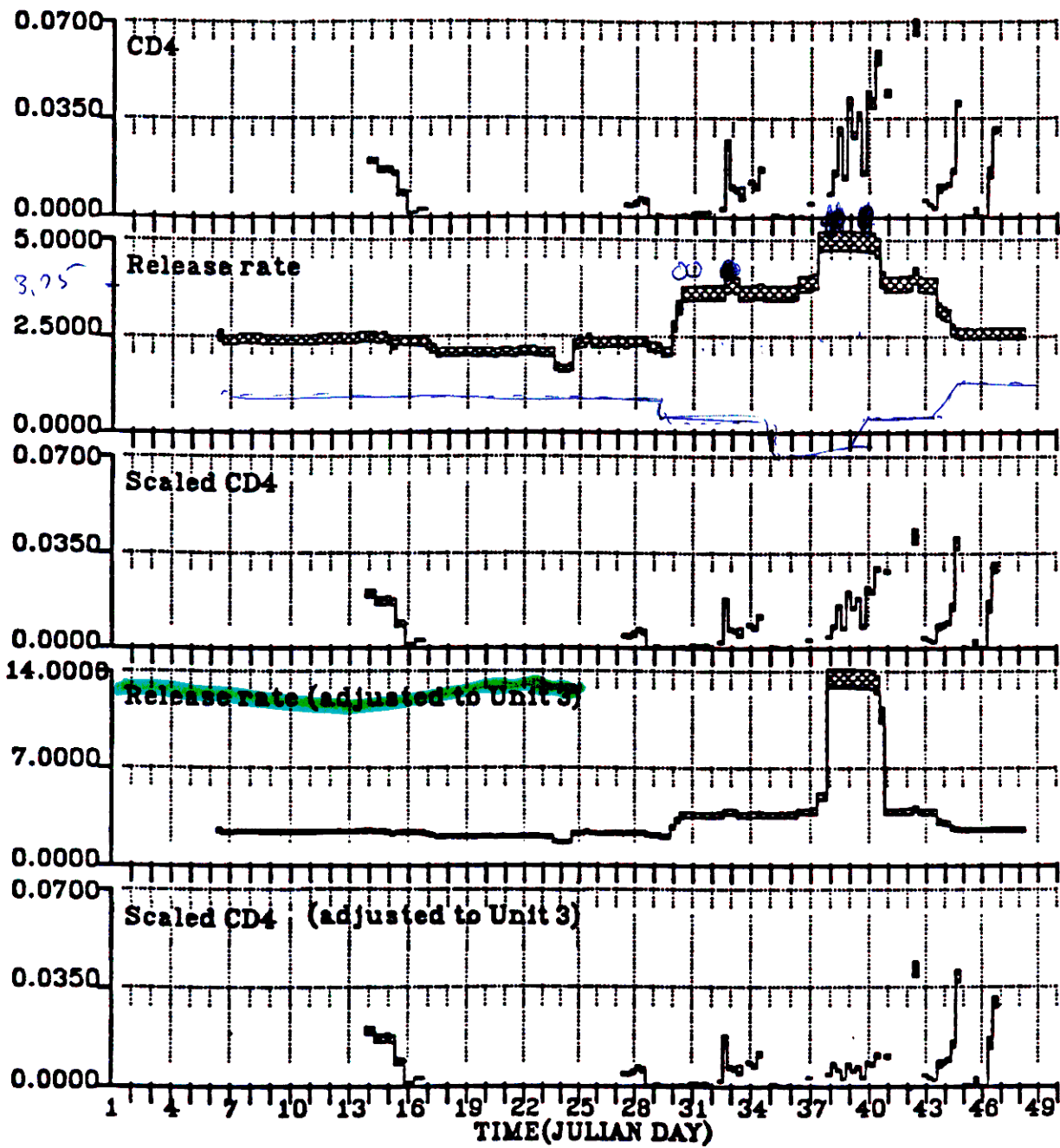


Figure 6.8:  $CD_4$  concentrations,  $CD_4$  release rate,  $CD_4$  concentrations scaled to release rate, apparent  $CD_4$  release rate accounting for Unit 3, and  $CD_4$  concentrations scaled to the apparent release rate at Page.

$$SCD_4 = CD_4 \times 2.5 / RR$$

$$= \frac{(S/CD_4)_S}{(S/CD_4)_G}$$

in dry deposition. Wesely<sup>2</sup> presents a detailed parameterization of the various elements that control dry deposition rates.

Dry deposition is commonly characterized by the deposition velocity  $v_d$  which is defined as follows:

$$v_d = F/C, \quad (6.1)$$

where  $F$  is the flux of material to the earth's surface and  $C$  is the ambient atmospheric concentration of the species.

The deposition velocity is inversely proportional to the sum of several resistances:

$$v_d = (r_a + r_b + r_c)^{-1}, \quad (6.2)$$

where  $r_a$  is the aerodynamic resistance between a specified height and the surface (common to all gases and a function of vertical atmospheric diffusion),  $r_b$  is the quasilaminar sublayer resistance (a function of the molecular diffusivity of the gas in air), and  $r_c$  is the bulk surface resistance.

Wesely<sup>2</sup> identifies the various components of  $r_c$  as shown in Figure 6.9 and in the following equation:

$$r_c = [1/(r_s + r_m) + 1/r_{lu} + 1/(r_{dc} + r_{cl}) + 1/(r_{ac} + r_{gs})]^{-1}, \quad (6.3)$$

where  $r_s$  is the resistance corresponding to the leaf stomata,  $r_m$  is the leaf mesophyll resistance,  $r_{lu}$  the leaf cuticle and upper canopy resistance,  $r_{dc}$  is the gas-phase canopy resistance,  $r_{cl}$  is the lower canopy leaf, bark and twig resistance,  $r_{ac}$  is the resistance of the canopy itself, dependent on canopy height and density, and  $r_{gs}$  is the ground surface resistance.

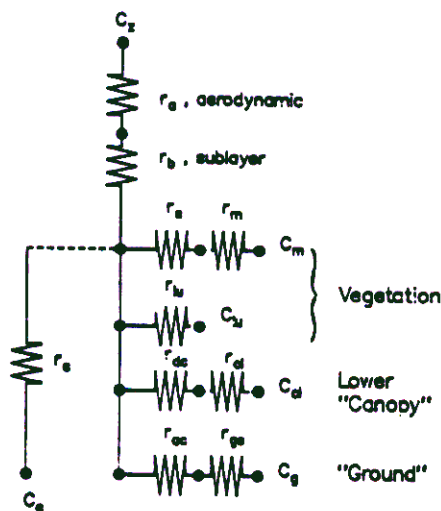


Figure 6.9: Combination of resistances that affect the total dry deposition velocity  $v_d$  (Source: Wesely, 1989).

In the most recent and sophisticated regional models,  $r_c$  is calculated internally as a function of the combined set of resistances for the specific surface conditions. However, in most situations measured values of  $v_d$  and  $r_c$  are used. The range of plausible dry deposition rates for  $SO_2$  and sulfate used in the DMB model, were literature values of measured  $v_d$ .

Tables 6.5 and 6.6 present the range of deposition velocities that have been measured for different surfaces for sulfur dioxide ( $SO_2$ ) and submicron particles such as sulfate ( $SO_4^{2-}$ ). Deposition

velocities for  $SO_2$  range from 0.1 to 2.3 cm/s, with a median value of 0.7 cm/s. Deposition velocities are generally highest during the day when atmospheric mixing is strongest and leaf stomata of vegetation are open. Deposition velocities for fine particles range from 0 to 1.0 cm/s, with a median value of 0.2 cm/s

### 6.3.2 $SO_2$ Oxidation

Most ambient sulfate ( $SO_4^{=}$ ) is produced from the oxidation in the atmosphere of emitted sulfur dioxide ( $SO_2$ ). Thus, the contribution of an  $SO_2$  source to ambient sulfate is dependent both on the  $SO_2$  emission rate and the rate at which  $SO_2$  is oxidized to sulfate. Oxidation rates can be determined either empirically from measurements or theoretically from chemical fundamentals. If empirically and theoretically derived oxidation rates are in agreement, greater confidence can be placed in the rates.

The TMBR analysis of WHITEX data, discussed in Section 6.6.1, indicates that data can be best fit by an oxidation rate which varies linearly with relative humidity such that:

$$k_c = C RH, \quad (6.4)$$

where  $k_c$ , in percent per hour, is the pseudo-first-order rate constant for  $SO_2$  oxidation to  $SO_4^{=}$ ,  $C$  is a constant, and  $RH$  is the relative humidity in percent. The DMB analysis (Section 6.6.2) also indicated that oxidation rates, especially during humid conditions, can be greater than 1 percent per hour.

In this section we assess whether there is empirical and theoretical support for an oxidation rate that is a linear function of relative humidity.

#### Empirical Studies of Sulfur Oxidation

Table 6.7 summarizes the ranges of  $SO_2$  oxidation rates measured in power plant plumes. The measured oxidation rates vary from 0 to 15 percent per hour. The mean of these reported rates is 3 percent per hour. The median of the lower bound is 0 percent per hour and the median of the upper bound is 5 percent per hour.

It should be noted that the oxidation rates in Table 6.7 may not be representative of the nonurban wintertime conditions for the WHITEX experiment. For example, it is known that gas-phase oxidation is faster during summer than in winter.

On the basis of empirical studies, a few generalities can be made regarding  $SO_2$  oxidation rates. Rates are faster:

- In summer than in winter
- In the day than at night
- In polluted atmospheres than in clean ones.
- In clouds and fog than in clear skies.

Oxidation rates in power plant plumes have ranged up to as high as about 10 percent per hour<sup>32, 33</sup>; however, much higher rates have been observed when a plume passes through a cloud or a fog bank.<sup>34</sup> At the Navajo Generating Station, Richards<sup>35</sup> measured maximum (noontime)  $SO_2$  oxidation rates of 0.8 percent per hour during the summer and 0.2 percent per hour in winter. The diurnal average rates were much lower than these maxima. However, all measurements were made

Table 6.5: Deposition velocities for  $SO_2$  for various types of surfaces (adapted from Hicks (1984)).

<u>Type of Surface</u>	<u>Deposition Velocity</u> <u><math>v_d</math> (cm/s)</u>	<u>Reference</u>
<u>Crops</u>		
Alfalfa (daytime)	2.3	Hill (1971) <sup>3</sup>
Wheat	0.4	Fowler (1978) <sup>4</sup>
Soybean	1.3	Fowler (1978) <sup>4</sup>
Wheat	0.4	Dannevik <i>et al.</i> (1976) <sup>5</sup>
<u>Grass</u>		
Pasture (daytime)	1.2	Garland <i>et al.</i> (1973) <sup>6</sup>
Pasture (daytime)	1.3	Owers and Powell (1974) <sup>7</sup>
Grass (daytime)	1.3	Shepherd (1974) <sup>8</sup>
Grass (autumn)	0.3	Shepherd (1974) <sup>8</sup>
Grass (daytime)	1.0	Whelpdale and Shaw (1974) <sup>9</sup>
<u>Soil</u>		
Calcerous soil	1.2	Garland (1977) <sup>10</sup>
<u>Trees</u>		
Pine plantation	0.1–0.6	Garland and Branson (1977) <sup>10</sup>
Pine plantation	< 1.0	Belot (1975) <sup>11</sup> as summarized in Chamberlain (1980) <sup>12</sup>
Pine forest	0.2	Galbally <i>et al.</i> , (1979) <sup>13</sup>
<u>Snow</u>		
	1.0	Whelpdale and Shaw (1974) <sup>9</sup>
	0.1	Dovland and Eliassen (1976) <sup>14</sup>
	0.2	Barrie and Walmsley (1978) <sup>15</sup>

Table 6.6: Deposition velocities for submicron particles (e.g., sulfate) for various types of surfaces (adapted from Hicks (1984)).

<u>Type of Surface</u>	<u>Deposition Velocity</u> <u><math>v_d</math> (cm/s)</u>	<u>Reference</u>
<u>Crops</u>		
	< 1.0	Droppo (1980) <sup>16</sup>
	0.1	Wesely and Hicks (1979) <sup>17</sup>
<u>Grass</u>		
	0.2	Sehmel <i>et al.</i> (1973) <sup>18</sup>
	0.2	Chamberlain (1960) <sup>19</sup>
	0.04	Hudson and Squires (1978) <sup>20</sup>
	0.9	Davidson and Friedlander (1978) <sup>21</sup>
	< 0.8	Wesely <i>et al.</i> (1977) <sup>22</sup>
	1.0	Everett <i>et al.</i> (1979) <sup>23</sup>
Unstable, light winds	0.4	Sievering (1982) <sup>24</sup>
Daytime	0.7	Hicks <i>et al.</i> (1982) <sup>25</sup>
Long-term average	0.2	Hicks <i>et al.</i> (1982) <sup>25</sup>
Daytime, lush grass	0.5	Wesely <i>et al.</i> (1982) <sup>26</sup>
Strongly stable, dry grass	0.2	Wesely <i>et al.</i> (1982) <sup>26</sup>
<u>Trees</u>		
	0.7	Hicks and Wesely (1978, 1980) <sup>27, 28</sup>
	> 0.6	Wesely and Hicks (1979) <sup>17</sup>
	> 0.1	Lindberg <i>et al.</i> (1979) <sup>29</sup>
	0	Wesely <i>et al.</i> (1982) <sup>26</sup>
<u>Snow</u>		
Stable conditions	0.16	Dovland and Eliassen (1976) <sup>14</sup>
<u>Water</u>		
Long-term average	0	Sievering <i>et al.</i> (1979) <sup>30</sup>
	0.2-1.0	Sievering <i>et al.</i> (1979) <sup>30</sup>
	< 0.05	Williams <i>et al.</i> (1978) <sup>31</sup>

during cloud-free conditions. At a coal-fired power plant in Alberta, Canada, Lulis et al.<sup>36</sup> reported  $SO_2$  oxidation rates of less than 0.5 percent per hour during the winter and in early morning in summer, but found rates of 1 to 3 percent per hour at midday in June. Noontime oxidation rates in a power plant plume were found to be 1 to 4 percent per hour, compared to nighttime rates of less than 0.5 percent per hour.<sup>37, 38, 39</sup> Rates of  $SO_2$  oxidation up to about 30 percent per hour have been observed in Budapest, Hungary<sup>40</sup> and in St. Louis.<sup>41, 42</sup>

Oxidation rates in clouds and fog banks appear to be much higher than rates in cloud-free air. Cass and Shair<sup>43</sup> observed  $SO_2$  oxidation rates of 4.5 to 10.8 percent in Los Angeles. They suggested aqueous-phase oxidation as a possible contributing factor to such high rates.

Finlayson-Pitts and Pitts<sup>44</sup> conclude as follows:

"In both plumes and ambient air, the presence of liquid water in aerosols, clouds, and fog is now accepted to be an important factor in determining the overall rate of conversion of  $SO_2$ . These water drops provide a medium in which aqueous phase reaction can occur and it is now believed that such condensed phase reactions contribute significantly to the  $SO_2$  oxidation under some conditions. For example, a 'burst of sulfate formation' has been observed in power plant plumes that pass through a cloud layer, and increased rates of  $SO_2$  conversion in such plumes are generally observed at higher relative humidities, >75%<sup>45, 46, 47, 32, 48, 34</sup> Similarly, in ambient air studies in the Ohio River Valley, evidence for significant production of both sulfuric and nitric acids in clouds was obtained.<sup>49</sup>"

On the basis of this empirical evidence, obtained largely at locations and during periods different from the WHITEX experiment, it appears that  $SO_2$  oxidation rates on the order of 1 percent per hour are plausible. Although the WHITEX experiment was carried out in a nonurban area in winter, when gas-phase reactions would tend to be slow, the period was characterized by high relative humidity, clouds, fog, and cooling tower plumes which would afford opportunities for relatively rapid aqueous phase  $SO_2$  oxidation.

### Theoretical Studies of Sulfur Oxidation

Gas-phase  $SO_2$  oxidation results primarily from the reaction with the hydroxyl radical ( $OH$ ). Hydroxyl radicals are formed from photochemical reactions involving ultraviolet light. Since ultraviolet flux is strongest when the sun is highest in the sky thus allowing less atmospheric filtering, gas-phase oxidation is fastest during the day and during summer. Although hydroxyl radical concentrations are enhanced in urban atmospheres where ozone and other photochemical reactants are more concentrated,  $OH$  can also be produced in nonurban settings such as the WHITEX experiment. The  $OH$  radical is produced primarily from the photodissociation of ozone, coupled with further reactions with water. Although ozone concentrations in the WHITEX study region range from 0.02 to 0.04 ppm, ultraviolet flux is relatively low because of the low sun angle and water vapor concentrations are low due to the low ambient temperatures. Latimer et al.<sup>50</sup> used a theoretical chemical mechanism for gas-phase  $SO_2$  oxidation that accounted for steady-state concentrations of  $OH$  and applied the model to a variety of seasons and times of day. Figure 6.10 shows the results of these calculations. Note that the modeled oxidation rates peak at noon and drop to zero at night. Rates are higher during the summer than during spring, fall, or winter. These calculated results agree well with the maximum (noontime) rate of 0.2 percent per hour measured by Richards et al.<sup>35</sup> in winter at the Navajo Generating Station. However, for summer the theoretical maximum is 1.5 percent per hour, versus a measured 0.8 percent per hour. The theoretical results are based on clear sky conditions. Significant clouds would tend to reduce ultraviolet flux. Also, if water

vapor concentrations or ozone concentrations were less than assumed, actual rates would be less than these calculations.

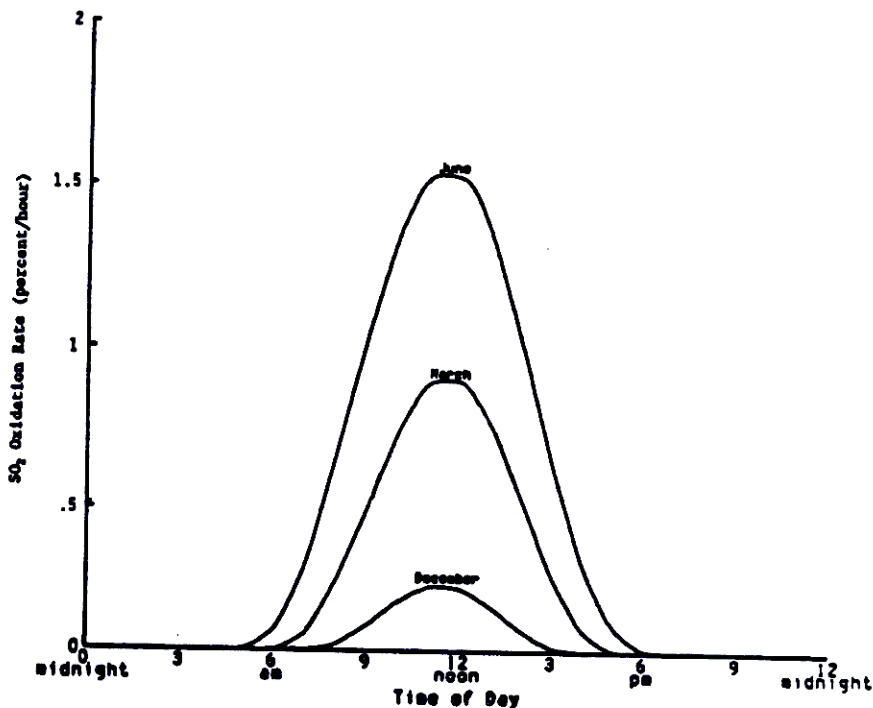


Figure 6.10: Calculated gas-phase  $SO_2$  oxidation rates as a function of time of day and season (Source: Latimer et al., 1985).

Perhaps the most important conclusion from Figure 6.10 is that gas-phase reactions simply are not fast enough to explain the  $SO_2$  oxidation rates on the order of 1 percent per hour suggested by WHITEX data. If one computes the 24-hour average  $SO_2$  oxidation rate from Figure 6.10 for winter, one obtains a value of approximately 0.03 percent per hour, a factor of 30 too low. Even the maximum gas-phase oxidation rate of 0.2 percent per hour is too low by a factor of 5.

Thus, these high oxidation rates can only be explained by aqueous-phase oxidation: reactions that occur within aerosols, or fog and cloud droplets. Theoretical calculations suggest that the higher rates observed during WHITEX are indeed plausible. Figure 6.11 shows the sulfur oxidation rates as a function of droplet pH as a result of reactions with ozone ( $O_3$ ), hydrogen peroxide ( $H_2O_2$ ), iron ( $Fe$ ), manganese ( $Mn$ ), carbon ( $C$ ), nitrous acid ( $HNO_2$ ), and nitrate nitrogen dioxide ( $NO_2$ ). All reactions, except the one with hydrogen peroxide, are strong functions of pH. As the droplet becomes more acidic (from production of sulfuric acid), oxidation is dramatically slowed. However, the reaction with  $H_2O_2$  remains rapid.

The reaction rates shown in Figure 6.11 are based on an assumed  $H_2O_2$  concentration of 1 *ppb*. Although  $H_2O_2$  concentrations were not measured during WHITEX, a series of measurements were made by Van Valin<sup>51</sup> during February 1987 along the 91.5 degree meridian from Iowa to the Gulf of Mexico. They found  $H_2O_2$  concentrations varied inversely with latitude, with values in the range from <0.1 to 1.0 *ppb*. At the latitude of the Grand Canyon (36 degrees), they found  $H_2O_2$  concentrations in the range from 0.1 to 0.6, centered on 0.3 *ppb*. They also found that  $H_2O_2$

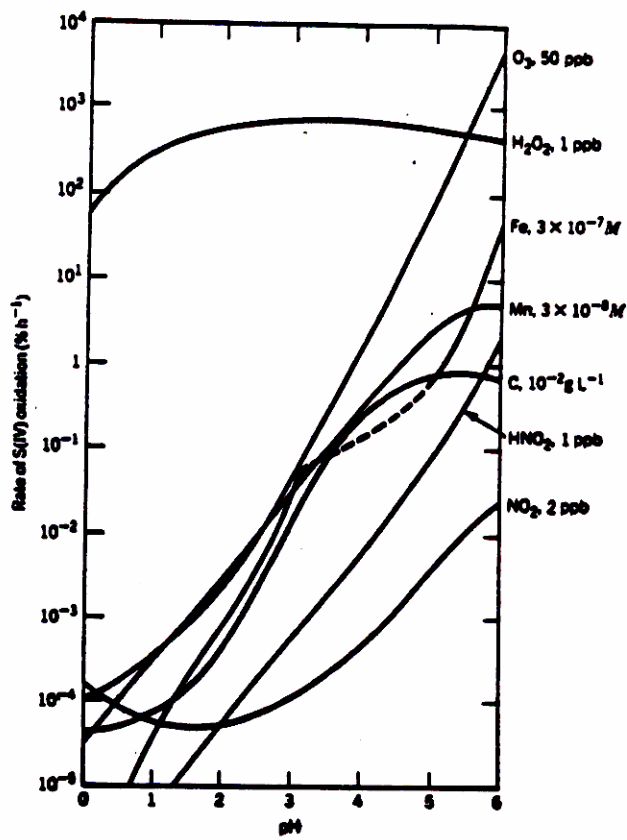


Figure 6.11: Calculated aqueous-phase  $SO_2$  oxidation rates as a function of droplet pH for assumed concentrations of oxidants (Source: Martin, 1984).

concentrations were dependent upon air mass history; air masses transported from lower latitudes generally had higher peroxide concentrations.

If we take the measured  $H_2O_2$  concentrations of Van Valin et al.<sup>51</sup> and scale the theoretical oxidation rates in Figure 6.11 down accordingly, we still have  $SO_2$  oxidation rates on the order of 100 percent per hour. Of course, such rates have not been observed during WHITEX or elsewhere because the  $H_2O_2$  is used up well before significant quantities of  $SO_2$  are oxidized. Since one mole of  $H_2O_2$  is consumed for each mole of  $SO_2$  oxidized, the average peroxide concentration of 0.3 ppb can produce  $0.4\mu g/m^3$  of sulfate as sulfur ( $1.2\mu g/m^3$  as sulfate). Of course higher concentrations of sulfate can be produced as additional  $H_2O_2$  is produced. Also, if the reactions with the other oxidants in Figure 6.11 are important, additional aqueous-phase oxidation could occur.

Thus, it appears that rapid  $SO_2$  oxidation suggested by the WHITEX data can be supported by theoretical aqueous-phase mechanisms. Although  $H_2O_2$  is not the only oxidant of importance, it has been measured at sufficient concentrations in winter to explain much of the observed sulfate formation. Iron and manganese, which are contained in NGS particulate matter, can catalyze the reaction with dissolved oxygen. Ozone, typically 20 to 40 ppb during the winter, can also contribute significantly to aqueous-phase oxidation.

Evidence for aqueous-phase oxidation is available in the particle size distribution data. When particle size distributions were stratified by relative humidity, a larger fraction of the total fine particle mass was in the  $0.5\mu m$  size range at the higher humidities. At lower humidities a relatively greater fraction of particles were found in the range 0.1 to  $0.3\mu m$ . Hering and Friedlander<sup>52</sup> found that sulfate in Los Angeles consisted of two sizes: (1) one at  $0.2\mu m$ , was found to be associated with sulfate formed from gas-phase oxidation and (2) one at  $0.5\mu m$  was found to be due to aqueous-phase oxidation. McMurry and Wilson<sup>53</sup> used aerosol growth data versus particle size to infer the relative importance of gas- and aqueous-phase oxidation mechanisms: growth in the  $0.5\mu m$  size range resulted mainly from aqueous-phase oxidation. Thus, the particle size data from WHITEX are consistent with the aqueous-phase oxidation mechanism.

The importance of aqueous-phase oxidation is indicated by the particle size data collected during WHITEX and the oxidation rates that are greater than what one would expect from gas-phase oxidation. While it is difficult to determine the relative importance of various aqueous-phase oxidants and catalysts, theoretical and empirical knowledge indicates that  $SO_2$  oxidation rates on the order of 1 percent per hour are plausible for aqueous-phase reactions, but not for gas-phase reactions. Thus, it is not surprising that the empirical fit of  $SO_2$  oxidation rate is proportional to relative humidity. The amount of water associated with hygroscopic aerosol increases with increasing humidity. Also, clouds, fog, and cooling tower plumes are more likely to occur at higher humidities.

## 6.4 Analysis of Meteorological Conditions

Upper-level winds from Page, Arizona were analyzed to determine possible NGS plume transport patterns. In addition, the ARL-ATAD backward air mass trajectory model was run for the western United States for the period of WHITEX to establish potential regional contributing source areas. Finally, the upper-level Page winds were used to calculate NGS plume parcel positions and ages as a function of time during the WHITEX experiment.

### 6.4.1 Summary of Upper-level Winds in Page

Table 6.8 summarizes the wind speed and direction measured at 300, 600, and 1000 meters above ground (m agl) for each of the soundings conducted during the WHITEX experiment. Typically,